CHEMISTRY OF MATERIALS

Article

pubs.acs.org/cm

Anatase TiO_2 Single Crystals Exposed with High-Reactive {111} Facets Toward Efficient H_2 Evolution

Hua Xu,[†,‡,§] Pakpoom Reunchan,[‡,∥] Shuxin Ouyang,*[,‡] Hua Tong,[⊥] Naoto Umezawa,[‡,⊥,#] Tetsuya Kako,[†,‡,§] and Jinhua Ye*[,†,‡,§,⊥]

[†]Graduate School of Chemical Science and Engineering, Hokkaido University, Sapporo 060-0814, Japan

[‡]Environmental Remediation Materials Unit and [§]International Center for Materials Nanoarchitectonics (WPI-MANA), National Institute for Materials Science (NIMS), 1-1 Namiki, Tsukuba 305-0044, Japan

[∥]Department of Physics, Faculty of Science, Kasetsart University, Bangkok 10900, Thailand

[⊥]TU-NIMS Joint Research Center, School of Materials Science and Engineering, Tianjin University, 92 Weijin Road, Nankai District, Tianjin 300072, P.R. China

[#]PRESTO, Japan Science and Technology Agency (JST), 4-1-8 Honcho Kawaguchi, Saitama 332-0012, Japan

Supporting Information

ABSTRACT: In this study, for the first time, {111} facet exposed anatase TiO_2 single crystals are prepared via both F^- and ammonia as the capping reagents. In comparison with the most investigated {001}, {010}, and {101} facets for anatase TiO_2, the density functional theory (DFT) calculations predict that {111} facet owns a much higher surface energy of 1.61 J/m^2, which is partially attributed to the large percentage of undercoordinated Ti atoms and O atoms existed on the {111} surface. These undercoordinated atoms can act as active sites in the photoreaction. Experimentally, it is revealed that this material exhibits the superior electronic band structure which can produce more reductive electrons in the photocatalytic reaction than those of the TiO_2 samples exposed with majority {010}, {101}, and {001} facets. More importantly, we demonstrate that this material is an excellent photocatalyst with much higher photocatalytic activity (405.2 μmol h^{-1}), about 5, 9, and 13 times that of the TiO_2 sample exposed with dominant {010}, {101}, and {001} facets, respectively. Both the superior surface atomic structure and electronic band structure significantly contribute to the enhanced photocatalytic activity. This work exemplifies that the surface engineering of semiconductors is one of the most effective strategies to achieve advanced and excellent performance over photofunctional materials for solar energy conversion.

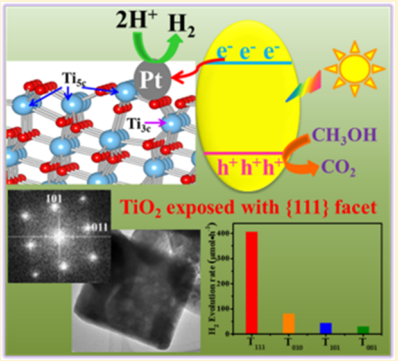

KEYWORDS: *anatase TiO_2, {111} facet, photocatalysis, surface chemistry*

INTRODUCTION

Photocatalysis is an environmentally friendly and promising technology to convert solar energy into chemical energy.[1−6] The discovery of water photolysis on TiO_2 electrode by Fujishima and Honda in 1972 was recognized as the landmark event in photocatalysis;[7] since then, large amounts of research have been carried out on TiO_2 photocatalysis to achieve a higher solar-to-energy conversion efficiency, such as modification of the electronic structure of TiO_2 to extend its light-absorption region via doping,[8,9] and fabrication of TiO_2-based heterojunction materials to enhance the charge separation efficiency.[10−13] Recently, special attention has been paid on the surface chemistry of TiO_2, since many physical and chemical processes (e.g., adsorption of reactant molecules, surface transfer of photoexcited electrons to reactant molecules, and desorption of product molecules) happened on the surface during the photocatalytic reaction.[14−16] Peculiarly, for a crystalline TiO_2, the surface geometric (atomic arrangement and coordination) and electronic structures vary with crystal facets in different orientations, leading to various physical and chemical properties.[17] Therefore, tailored synthesis of TiO_2 single crystals with optimized reactive facets is highly desirable for promoting the photocatalytic activity.

In the case of anatase TiO_2, the shape of this material under equilibrium conditions is a slightly truncated tetragonal bipyramid enclosed with 94% of {101} surfaces (the most thermodynamically stable) and minor {001} surfaces based on the Wulff construction and theoretically calculated surface energy ({101} (0.44 J/m^2) < {010} (0.53 J/m^2) < {001} (0.90 J/m^2)).[18] Nevertheless, in the real experimental process, the facet control of anatase TiO_2 can be effectively achieved.[19] A significant breakthrough was carried out by Yang and his co-workers, who experimentally obtained the anatase TiO_2 single crystals with majority of {001} facets.[20] Moreover, in spite of that no {010} facet can be observed in the Wulff construction model, the latest investigations have confirmed the existence of

Received: October 30, 2012
Revised: January 1, 2013

   dx.doi.org/10.1021/cm303502b | *Chem. Mater.* XXXX, XXX, XXX−XXX

{010} facet existed as the 'belt' at the center of TiO_2 particle.[21−24] Among these three crystal facets ({010}, {101}, and {001} facets), {001} facet was ever been considered to be the active facets in the photocatalysis because of its highest surface energy (0.90 J/m^2) and superior surface atomic structure (100% five-coordinated Ti atoms (Ti_{5c}) on its surface). However, in 2011, Pan et al. reported that {010} facet owns the superior electronic structure than that of {001} and {101} facets, and TiO_2 single crystals exposed with more {010} facets exhibited superior electronic band structure than that of TiO_2 exposed with more {001} facets, thus resulted into a much higher photocatalytic activity in the H_2 evolution.[17] Those above findings indicated that both the surface atomic structure and electronic structure play important roles in the photocatalytic reaction, thus inspire us to make TiO_2 expose new active crystal facet with superior properties in both atomic structure and electronic configuration. We expect that those unique properties can endow TiO_2 with high photocatalytic activity, hence promoting their potential applications in the clean energy and environmental remediation.

To date, compared with the previously investigated {001}, {101}, and {010} facets for anatase TiO_2, few studies have been concerned on the {111} facet, as illustrated in Scheme 1.

Scheme 1. Schematic Illustration of {101}, {010}, {001}, and {111} Facets of Anatase TiO_2: (a) Molecular Simulation Model; (b) Crystal Model

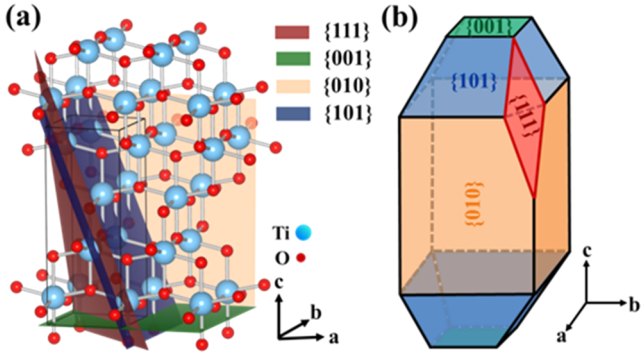

Herein, we report a facile process to prepare well-defined anatase TiO_2 single crystals exposed with {111} facets (T_{111}) which have never been realized experimentally before. The DFT theoretical calculations predict that the surface energy of {111} facet is up to 1.61 J/m^2 and large percentages of undercoordinated Ti atoms and O atoms existed on the surface. Experimentally, it is discovered that the conduction band minimum of this material is much higher than those of TiO_2 samples exposed with dominant {010}, {101}, and {001} facets (denoted as T_{010}, T_{101}, and T_{001}), indicating that more reductive electrons can be produced on T_{111} then take part in the photoreaction to reduce H^+ into H_2. Furthermore, the photocatalytic properties of T_{111} are evaluated, it is revealed that T_{111} is an excellent photocatalyst with much higher photocatalytic activity, about 5, 9, and 13 times that of T_{010}, T_{101}, and T_{001}, respectively. Both the superior surface atomic structure and electronic band structure significantly contribute to the enhanced photocatalytic performance. The previous research reported that {010} facet was the most active facet for anatase TiO_2, which owns 100% Ti_{5c} atoms on its surface and superior electronic structure compared to that of {101} and {001} facets.[17] However, in this study, {111} facet is proved to be the more active crystal facet than {010} facet, which exhibits excellent properties in both the surface atomic structure and electronic structure. To the best of our knowledge, it is the first report about the {111} facet exposed anatase TiO_2.

EXPERIMENTAL SECTION

Synthesis. In a typical synthesis procedure of TiO_2 single crystals exposed with {111} facet, first, 3 mmol of TiF_4 (Aldrich) was added into the 100 mL of mixed solution of ethanol (Wako) and acetonitrile (Wako); then 0.6 mL of ammonia (Wako) was added slowly into the above solution. After being stirred at room temperature for 48 h, the white suspension was centrifugated and the followed precipitation was dried at 60 °C for 3 h to get the gel-like precursor (denoted as TFN). To get the final single-crystalline TiO_2, we heated the Ti precursor (TFN) at 500 °C for 2 h with a temperature ramping rate of 1 °C/min in the air atmosphere. After the combustion process, loosely TiO_2 powder was obtained. Furthermore, the obtained samples need to be calcined in the air atmosphere at 600 °C for 2 h to clean the surface for the photocatalytic test. This as-prepared TiO_2 sample was denoted as T_{111}.

In comparison with T_{111}, TiO_2 samples with exposed {001}, {010}, and {101} facets were prepared via solvothermal method reported in the literature as following:[17] 64, 32, 32 mg of titanium oxysulfate ($TiOSO_4.xH_2O$) (Aldrich) was dissolved in the HF solution (Aldrich) with concentrations of 120, 40, and 80 mM to prepare the precursors of TiO_2 with {001}, {010}, and {101} facet exposed, respectively. Then 40 mL of the $TiOSO_4$ solution were transferred to the Teflon-lined autoclave and heated at 180 °C for 12, 2, and 12 h for the {001}, {010}, and {101} facet exposed TiO_2, respectively. After reaction, the products were collected by centrifugation and washed with deionized water then dried at 80 °C in air for 12 h. To remove the surface fluorine, all the products were calcined in the air atmosphere at 600 °C for 2h. The samples with {001}, {010}, and {101} facets exposed were denoted as T_{001}, T_{010}, and T_{101}, respectively.

Characterization. The X-ray diffraction (XRD) patterns of the prepared samples were conducted on a Rigaku Multiflex diffractometer (RINT 2000; Rigaku Corp., Japan) with monochromatized Cu K_a radiation (λ=1.54178 Å). Raman measurement was carried out using a Raman spectroscopy (NRS-1000; Jasco Corp. Japan). The size and morphology of the samples were observed with a scanning electron microscope (SEM, JSM-6701F, JEOL Co., Japan) and transmission electron microscope (TEM, JEM-200 CX, JEOL) operating at 200 kV. The low temperature Electron Paramagnetic Resonance (EPR) spectra of the TiO_2 samples were recorded at 4 K to confirm the presence of oxygen vacancy on JEOL JES-FA200 Electron Spin Resonance Spectrometer. UV−visible absorption spectra were measured on a UV−visible spectrophotometer (UV-2500PC, Shimadzu Co., Japan). X-ray Photoelectron Spectroscopy (XPS) were performed on Thermo ESCALAB250 using monochromatized Al K_a at $h\upsilon$ = 1486.6 eV. The binding energies were calibrated to the C_{1s} peak by 284.6 eV. The Brunauer−Emmett−Teller (BET) surface areas were recorded by a surface area analyzer (BEL Sorp-II mini, BEL Japan Co., Japan) with nitrogen absorption at 77 K.

Theoretical Calculations. The calculations of the surface structure were based on the density-functional theory (DFT), as implemented in the VASP code.[25] The exchange-correlation energy was represented by the generalized-gradient approximation (GGA) of Perdew, Burke, and Ernzerhof (PBE).[26] The Ti $3s^23p^63d^24s^2$ and O $2s^22p^4$ were treated as valence electrons. The energy cutoff for the plane-wave basis set was 400 eV. The calculated crystal parameters for bulk anatase TiO_2 were a = 3.786 Å and c/a = 2.556, which were in good agreement with the experimental values.[27] A 6 × 6 × 6 Monkhorst k-point mesh was used for the Brillouin-zone integrations of the unit cell. For each surface, the supercells which were constructed from the relaxed unit cell of TiO_2 were periodically repeated along the surface normal and separated by vacuum layers. The constructed slabs with a vacuum thickness of ~10 Å can sufficiently suppress the interaction between adjacent slabs. The surface models were consisted of 144 atoms (24 unit cells of bulk TiO_2) for {111} and {001} planes,

dx.doi.org/10.1021/cm303502b | Chem. Mater. XXXX, XXX, XXX−XXX

and 96 atoms (16 unit cells) for {010} and {101} planes, respectively. All atoms in the slabs were relaxed until the residual force was less than 0.02 eV/Å.

To further investigate the possibility of the oxygen vacancy existed on each surface, we also calculated the surface energies of the reduced surfaces. In the model structure, one oxygen atom was removed from each side of the {101}, {010}, {001}, and {111} slabs mentioned above. The geometries of the reduced surfaces were fully relaxed. The surface energy γ' of the reduced surface was given by

$$\gamma' = \frac{E_{\text{slab}}^{\text{reduced}} - nE_{\text{bulk}}}{2A} + \frac{\mu_o}{A}$$

, where $E_{\text{slab}}^{\text{reduced}}$ is the total energy of the reduced slab, and μ_o is the chemical potential of oxygen, which is directly related to the O_2 partial pressure in ambient.

Photocatalytic Test. Photocatalytic reactions of H_2 evolution were carried out in a closed gas circulation system with an external-irradiation type of a glass reactor. The light source was a 300 W xenon lamp. The intensity of the light at 300−800 nm was measured to be 240 mW/cm^2 by using a spectroradiometer (USR-40; Ushio Inc., Japan). The cocatalyst Pt was loaded by an in situ photodeposition method. The 0.5 wt % Pt-loaded catalyst (60 mg) was dispersed with a magnetic stirrer in an aqueous methanol solution (50 mL of CH_3OH and 220 mL of H_2O). The evolved gas including H_2 was analyzed by an online gas chromatograph (GC-8A; Shimadzu) equipped with a thermal conductivity detector.

RESULTS AND DISCUSSION

As shown in Figure 1, the XRD patterns of the as-prepared TiO_2 samples (T_{001}, T_{101}, T_{010}, and T_{111}) can be indexed to the

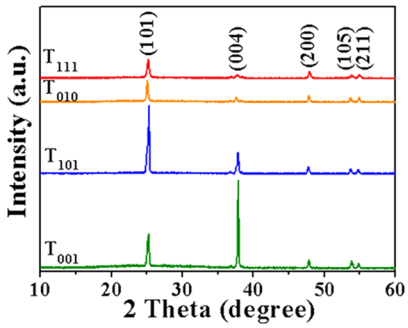

Figure 1. XRD patterns of the TiO_2 samples (T_{001}, T_{101}, T_{010}, and T_{111}).

anatase TiO_2 (JCPDS No. 84−1286). The diffraction peaks at 25.32, 37.93, 48.02, 53.98, and 55.04° are corresponding to the (101), (004), (200), (105), and (211) planes of anatase TiO_2, respectively. The differences in the peak intensity at 25.32° (101) and 37.93° (004) for the four TiO_2 samples are mainly related to the preferential crystallographic orientation of the crystal facets exposed. However, no corresponding characteristic peak for {111} facet can be observed in the XRD patterns. Structurally, anatase TiO_2 crystallizes in a tetragonal lattice, belonging to the space group of $I4_1/amd$. Only in the case of $h + k + l = 2n$ (n = 1, 2, 3, ...), the diffraction peak will occur in the XRD pattern, thus the absence of (111) crystal plane is resulted from the extinction rules in the X-ray diffraction measurements.[27]

To further confirm the TiO_2 samples were pure anatase, we measured the Raman spectra to identify the crystal structure of all the four prepared TiO_2 samples. As shown in Figure S1 in the Supporting Information, the peaks appeared at 396, 515, and 638 cm^{-1} are corresponding to the B_{1g}, A_{1g}, and E_g peaks of anatase TiO_2, respectively.[28] Obviously, the peak positions of all the four prepared TiO_2 samples (T_{111}, T_{010}, T_{101}, and T_{001}) are similar, no other additional peaks indexed to rutile can be found. Therefore, we can prove that all the four prepared TiO_2 samples (T_{111}, T_{010}, T_{101}, and T_{001}) are pure anatase.

The morphology of the TiO_2 sample (T_{111}) was observed by the SEM image (Figure 2a), which was consisted of some

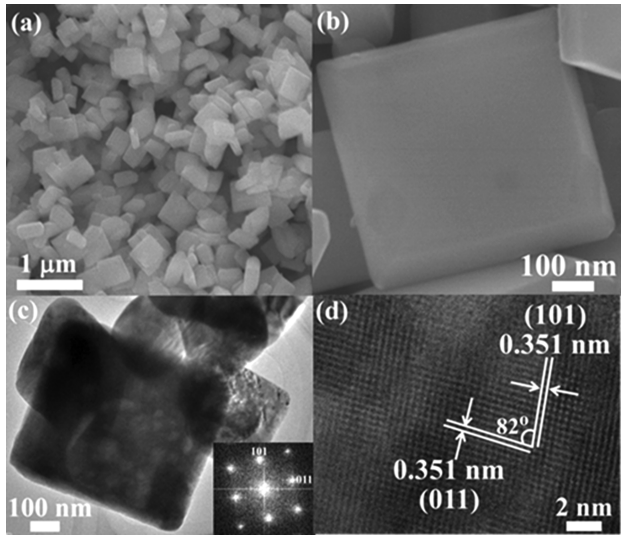

Figure 2. (a, b) SEM, (c) TEM, and (d) HRTEM images of the single-crystalline TiO_2 exposed with {111} crystal facets.

square-like plates. As shown in Figure 2b, a square-shaped plate (400 × 400 nm^2) with a thickness of 50 nm in high-magnification was observed. Furthermore, a detailed study was carried out to verify the crystal facet of the square-shaped nanoplates via TEM (Figure 2c). The corresponding electron diffraction (SAED) pattern (inset in Figure 2c) confirms that the square-shaped crystalline is single crystal, and the zone axis is indexed to be [111]. Additionally, based on the analysis of the high-resolution TEM (HRTEM) image (Figure 2d), the interfacial angle between the (101) and (011) atomic planes (the same lattice spacing of 0.351 nm) of anatase TiO_2 is 82°, we can confirm that the exposed crystal plane is {111} facet. To the best of our knowledge, this is the first report about the single crystalline TiO_2 with {111} facet exposed. According to the SEM and TEM images, the percentage of the {111} facets on T_{111} is calculated to be about 72% in average. For the morphology observation of other TiO_2 samples (T_{001}, T_{101}, and T_{010}), the SEM images are shown in Figure S2 in the Supporting Information.

On the basis of the above experimental findings, the surface structure of the {111} crystal facet was further theoretically studied via the density functional theory (DFT) calculation in comparison with the reported {001}, {010}, and {101} facets. The representative relaxed atomic geometries of each slab are shown in Figure 3. Accounting from the slab models, the surface atomic structures of each facets are described as following. On the {111} surface, all the Ti and O atoms on the top layer are undercoordinated: Ti atoms are 5-fold and 3-fold coordinated (Ti_{5c} and Ti_{3c}) with the ratio of Ti_{3c} to Ti_{5c} is 1:3, and O atoms are 2-fold coordinated (O_{2c}). On the {001} surface, only Ti_{5c} atoms are present as well as O_{2c} and O_{3c} atoms. On the {010} surface, we note that besides the outmost Ti_{5c} atoms on the top layer, the fully (6-fold)-coordinated Ti

dx.doi.org/10.1021/cm303502b | Chem. Mater. XXXX, XXX, XXX−XXX

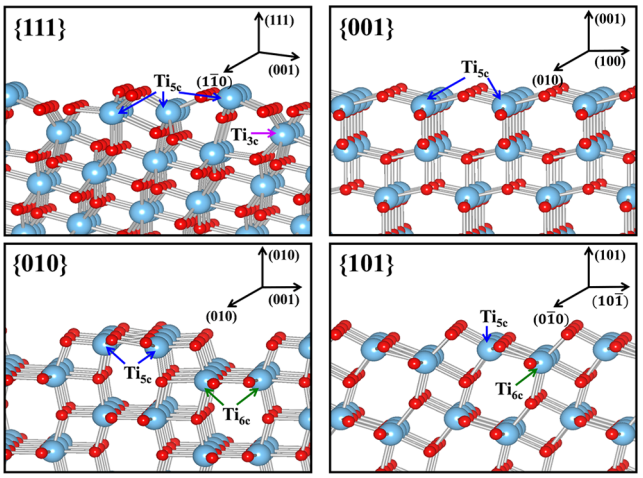

Figure 3. Surface structures of the relaxed stoichiometric {111}, {001}, {010}, and {101} facets.

(Ti_{6c}) atoms are also exposed on the second layer. In addition, both O_{2c} and O_{3c} atoms are existed on the surface of {010}. On the {101} surface, both Ti_{6c} and Ti_{5c} atoms are present as well as O_{2c} and O_{3c} atoms. Apparently, {111} surface has favorable atomic structure, on which the large percentage of undercoordinated Ti atoms (Ti_{5c} and Ti_{3c}) can act as the active reaction sites in the photocatalytic reaction.[29,30]

Meanwhile, the surface energy (γ) of each facet was calculated by the formula

$$\gamma = \frac{E_{slab} - nE_{bulk}}{2A}$$

, where E_{slab} is the total energy of the slab, E_{bulk} is the total energy of the bulk per unit cell, n is the number of bulk unit cells contained in the slab, and A is the surface area of each side of the slab. The calculated surface energies are 1.61, 0.95, 0.57, and 0.43 J/m^2 for {111}, {001}, {010}, and {101} facets, respectively; the latter three surface energies are in well accordance with the values reported in the literature (as listed in Table 1).[18] However, to the best of our knowledge, the surface energy of {111} facet has never been reported. Compared with {001}, {010}, and {101} facets, the surface energy of {111} facet is much higher. The higher surface energy of {111} facet is partially attributed to the large percentage of undercoordinated Ti and O atoms, of which the ground state energy is higher in contrast with the fully coordinated atoms.

Table 1. Surface Energies of Each Crystal Facet for Anatase TiO_2

crystal facet	surface energy (J/m^2) this work	surface energy (J/m^2) GGA-PBE[18]
{101}	0.43	0.44
{010}	0.57	0.53
{001}	0.95	0.90
{111}	1.61	

Generally, the facet with high surface energy will vanish rapidly during the crystal growth process to minimize the total crystal energy. In order to stabilize the reactive surface during the crystal growth process, the TiO_2 samples with exposed high-energy {001} and {010} facets were prepared by using HF,[17,20,31−40] NH_4F,[19,41,42] or any other capping reagents (such as 1-butyl-3-methylimidazolium tetrafluoroborate,[38,43] disodium ethylenediaminetetraacetate,[44] and diethylenetriamine[45]) as stabilizers to lower the surface energy for certain crystallographic crystal facets in the previous report.[46] Herein, anatase TiO_2 single crystals with high-surface-energy {111} facet exposed is obtained, which could be ascribed to the synergetic effect of the F^- and ammonia as the capping reagents. The crystal growth mechanism was also investigated in detail as described in the Supporting Information (Figures S3 and S4).

In addition, the numerous undercoordinated O atoms (100% O_{2c}) existed on the {111} surface can facilitate the formation of oxygen vacancy, which will affect the photocatalytic performance via acting as active sites in the photoreaction.[47] In order to verify the possibility of the existence of oxygen vacancy existed on the TiO_2 surface, the surface energy of the reduced {111} surface was theoretically calculated in comparison with other crystal facets such as {001}, {010}, and {101}. As shown in Figure S5a in the Supporting Information, the intersection of the ideal and reduced surface curves gives the transition value of ∼ −1.61 eV for the {111} facet, which is much higher than that of the {001} (approximately −3.76 eV), {010} (approximately −4.25 eV), and {101} (approximately −4.52 eV) facets. These results indicate that the oxygen vacancies can be more easily created on the {111} surface than that on the {001}, {010}, and {101} surfaces, and oxygen vacancies start to form on the {111} surface even under a relatively high O_2 pressure.[15] Later, to get a more convincing experimental evidence, we also adopted the low temperature electron paramagnetic resonance (EPR) spectra to check the existence of the oxygen vacancies on the TiO_2 surface. As shown in Figure S5b in the Supporting Information, the signal observed at g = 2.002 is the characteristics of a paramagnetic Ti^{3+} existed on the surface of TiO_2. It is reported that the surface Ti^{3+} would tend to adsorb atmospheric O_2, and reduce the O_2 into O_2^-, which shows an EPR signal at g = 2.002.[48] The intensity of the signal appeared in T_{111} is much stronger than that of T_{010}, T_{101}, and T_{001}, indicating that more oxygen vacancies are existed on the surface of T_{111}. These oxygen vacancies can act as active sites in the photocatalytic reaction, which are beneficial for the enhancement of the photocatalytic efficiency.

In parallel, the electronic band structures of the four TiO_2 samples, which will also affect their photocatalytic efficiencies, were deduced from the UV−visible absorption spectra and valence band XPS spectra. As shown in Figure 4a, the UV−visible absorption spectra demonstrate that, the absorption edges of T_{111}, T_{010}, T_{101}, and T_{001} are nearly 371, 385, 388, and 392 nm, respectively. TiO_2 is known as an indirect semiconductor, for which the relation between the absorption coefficient (a) and incident photon energy ($h\nu$) can be written as $a = B_i(h\nu - E_g)^2/h\nu$, where B_i is the absorption constant for indirect transitions.[49] The band gaps of the TiO_2 samples are calculated to be 3.01, 3.04, 3.08, and 3.17 eV for T_{001}, T_{101}, T_{010}, and T_{111}, respectively (Figure 4b). Because each facet owns its own unique surface atomic arrangement, which will result in different electronic configuration from other facet, thus TiO_2 single crystals exposed with various crystal facets will exhibit different electronic band structures.[17,23] As shown in Figure 4c, the valence band XPS spectra reveal that the VB maxima of all the four TiO_2 samples are similar. Consequently, the order of the potential of the conduction band minimum are $T_{111} > T_{010} > T_{101} > T_{001}$ (Figure 4d). In the photocatalytic reaction, considering the effect of the electronic band structure, the TiO_2 sample with a higher conduction band minimum which can generate more reductive electrons to take part in the

dx.doi.org/10.1021/cm303502b | Chem. Mater. XXXX, XXX, XXX−XXX

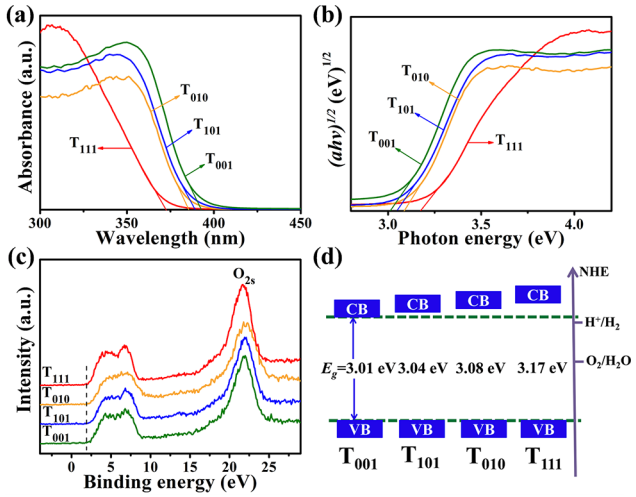

Figure 4. (a) UV−visible absorption spectra of the TiO_2 samples. (b) Their corresponding plots of transformed Kubelka−Munk function versus the energy of photon. (c) Valence-band XPS spectra of the four TiO_2 samples. (d) Schematic illustration of the determined valence-band (VB) and conduction-band (CB) edges of T_{001}, T_{101}, T_{010}, and T_{111}.

photocatalytic reaction will show superior photocatalytic activity.[50] Hence, among these four TiO_2 samples, T_{111} possesses a superior electronic band structure, in which more strongly reductive electrons can be generated, then transferred to the TiO_2 surface to take part in the photocatalytic reaction.

Furthermore, the photocatalytic H_2 evolution from an aqueous methanol solution was employed for evaluation of the photocatalytic property of T_{111} as well as the other TiO_2 samples (T_{010}, T_{101}, and T_{001}). As shown in Figure 5a, T_{111}

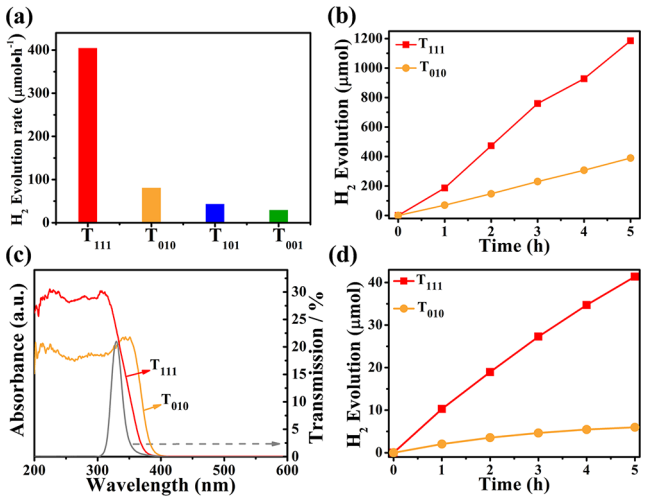

Figure 5. (a) Photocatalytic water splitting tests of the Pt-loaded (0.5%) TiO_2 samples with the same mass of 60 mg under UV−visible light irradiation (λ > 300 nm). (b) Comparison of photocatalytic activities between T_{111} (20 mg × 11.6 m^2/g = 0.232 m^2) and T_{010} (60 mg × 3.96 m^2/g = 0.237 m^2) with same surface area (ca. 0.23 m^2) under UV−visible light irradiation (λ > 300 nm). (c) UV−visible absorption spectra of T_{111} and T_{010}, and the light transmission spectrum of the monochromatic filter centered at a wavelength of 327.5 nm ($\Delta\lambda$ = ±18.5 nm) (gray curve). (d) Comparison of photocatalytic activities between T_{111} and T_{010} with the same surface area of ca. 0.23 m^2 under the monochromatic light irradiation λ = 327.5 nm ($\Delta\lambda$= ±18.5 nm).

exhibits obviously higher photocatalytic activity with the H_2 evolution rate of 405.2 μmol h^{-1}, about 5 times that of T_{010} (81.1 μmol h^{-1}), 9 times that of T_{101} (43.9 μmol h^{-1}), and 13 times that of T_{001} (29.9 μmol h^{-1}). Among them, although Ti_{5c} is exposed 100% on the {001} surface and the surface energy of {001} facet is the second highest, the photocatalytic activity of T_{001} is the lowest. The low photocatalytic performance is resulted from its poor electronic band structure, which has been explained in detail in the previous report.[17] Herein, in this study, we only compared the photocatalytic performance between T_{111} and T_{010} (T_{010} was the most efficient photocatalyst in the previous study).

In general, the photocatalytic activity can be affected by various factors, such as crystallinity and surface area.[51] In this study, the crystallinity of the TiO_2 samples is hard to identify via the XRD patterns because of the preferential crystallographic orientation of each crystal facet. However, both T_{111} and T_{010} were heated at 600 °C in a static air atmosphere for 2 h to clean the surface before the photocatalytic test, thus the effect of crystallinity can be ignored based on the same calcination temperature. Moreover, considering the surface area, the Brunauer−Emmett−Teller (BET) specific surface areas are 11.6 and 3.96 m^2/g for T_{111} and T_{010}, respectively (see Table S1 in the Supporting Information). Taking the surface area into account, based on the data from Figure 5a, the photocatalytic activities are calculated to be 582.1 and 341.3 μmol h^{-1} m^{-2}) for T_{111} and T_{010}, respectively. In addition, we also experimentally tested the photocatalytic performance of the two photocatalysts (T_{111} and T_{010}) in the same surface area of ca. 0.23 m^2 (Figure 5b). In this case, the photocatalytic activity of T_{111} is about 3 times that of T_{010} as shown in Figure 5b. Therefore, on the basis of the above analysis, both the calculation and experimental results confirm that T_{111} exhibits higher specific activity than that of T_{010}.

Moreover, we should consider that the light absorption abilities for the two photocatalysts (T_{111} and T_{010}) under the UV−visible light irradiation are different (Figure 5c). The number of the absorbed photons between 300 and 400 nm were calculated to be 0.254 μmol/s and 0.367 μmol/s for T_{111} and T_{010}, respectively, via the method reported in our previous study.[52] It is apparent that the absorbed photons for T_{010} are approximately 1.5 times that of T_{111}. Hence, their photocatalytic performances under monochromatic light centered at a wavelength of 327.5 nm ($\Delta\lambda$ = ±18.5 nm) were also studied. As shown in Figure 5c, the light-absorption difference between T_{111} and T_{010} can be eliminated under this condition. In this way, it is worthy of note that T_{111} still exhibits a significantly higher photocatalytic activity (8.2 μmol h^{-1}), more than 6 times that of T_{010} (1.2 μmol h^{-1}) (Figure 5d).

Finally, to investigate the contribution of oxygen vacancy worked on the enhancement of the photocatalytic activity, control experiments related to the oxygen vacancy on T_{111} surface have been done. Instead of treating T_{111} into air atmosphere at 600 °C to clean the surface, we treated T_{111} into the pure O_2 atmosphere at 600 °C to obtain the oxygen-vacancy-free sample (denoted as T_{O_2}). The EPR spectra confirm that there is almost no oxygen vacancy existed on the T_{O_2} surface (see Figure S6a in the Supporting Information). T_{O_2} exhibits a slightly better crystallinity (see Figure S6b in the Supporting Information) and similar light absorption edge (see Figure S6c in the Supporting Information) to that of T_{111}. However, as shown in Figure S6d in the Supporting

dx.doi.org/10.1021/cm303502b | Chem. Mater. XXXX, XXX, XXX−XXX

Information, it is revealed that the photocatalytic activity of T_{O_2} without oxygen vacancy is only 0.75 times of T_{111} with small amount of oxygen vacancies, proving that the suitable amounts of oxygen vacancy existed on the T_{111} surface is indeed beneficial for the promotion of the photocatalytic performance.

On the basis of the above theoretical analysis and experimental results, we can address that the vital factor for the higher photocatalytic performance of T_{111} is the superior surface properties owned by {111} facet. Because of its particular surface structure, the surface atomic coordination and arrangement of {111} facet are obviously different from other facets (Figure 3). Accordingly, TiO_2 sample with dominant {111} facet exposed exhibited good candidate characters in both surface atomic structure (the density of undercoordinated atoms) and electronic band structure for the excellent photoreactivity, which can be explained in detail as following.

The first property relevant to the photocatalytic activity is the surface atomic structure. It is reported that a facet with a higher percentage of undercoordinated atoms are usually more reactive in the heterogeneous reactions. These undercoordinated Ti atoms on the TiO_2 surface can act as the catalytically active sites for the photoreaction.[53,54] On the {111} surface, all Ti atoms are undercoordinated (25% Ti_{3c} and 75% Ti_{5c}). Compared with {010} (100% Ti_{5c}), {001} (100% Ti_{5c}), and {101} (50% Ti_{5c} and 50% Ti_{6c}), the photoreactivity of {111} surface is thus expected to be higher than those of other facets. What's more, the formation of oxygen vacancies on the {111} surface, which is facilitated by the presence of numerous undercoordinated O atoms (100% O_{2c}), can also offer more active sites on the {111} surface, thus enhance the photocatalytic activity.[47] Another key issue influencing the photocatalytic efficiency is the electronic band structure. On the basis of the deduced electronic band structures of the four TiO_2 samples (T_{111}, T_{010}, T_{101}, and T_{001}), the conduction band minimum of T_{111} is the highest, hence the more strongly reductive electrons can be produced then transferred to the surface Pt sites to reduce H^+ into H_2.[50] Thereby, compared with the previous report in which the photoreactivity only can be promoted by one or two times via facet control,[17] herein, via optimizing both the surface atomic structure and electronic band structure, T_{111} exhibits the obviously higher photocatalytic activity, about five times that of T_{010} (Figure 5a).

CONCLUSIONS

The well-defined {111} facet exposed TiO_2 single crystals are synthesized via both F^- and ammonia as the capping reagents. This TiO_2 sample exhibits an obviously higher photocatalytic activity in comparison to TiO_2 samples exposed with majority {001}, {101}, and {010} facets. The largely enhanced photocatalytic activity can be attributed to its superior surface atomic structure (large percentage of undercoordinated atoms on the TiO_2 surface to act as the active sites for the photoreaction) and electronic band structure (higher conduction band minimum on which more reductive electrons can be generated). This fundamental understanding shows that the facet control of semiconductors allows the optimization of both the surface atomic structure and electronic band structure, thus largely promotes the photocatalytic efficiency. This study evidence that the surface-structural engineering of semiconductors is an effective approach to achieve advanced and excellent performance over photocatalysts.

ASSOCIATED CONTENT

Supporting Information

Raman spectra, SEM image, control experiments for the study of formation mechanism, investigations about the oxygen vacancy. This material is available free of charge via the Internet at http://pubs.acs.org.

AUTHOR INFORMATION

Corresponding Author

*Tel.: 81-29-859-2646. E-mail: Jinhua.YE@nims.go.jp (J.Y.); OUYANG.Shuxin@nims.go.jp (S.O.).

Notes

The authors declare no competing financial interest.

ACKNOWLEDGMENTS

This work was partially supported by World Premier International (WPI) Research Center Initiative on Materials Nanoarchitectonics (MANA), MEXT, and the Japan Science and Technology Agency (JST) Precursory Research for Embryonic Science and Technology (PRESTO) program.

REFERENCES

(1) Yi, Z. G.; Ye, J. H.; Kikugawa, N.; Kako, T.; Ouyang, S. X.; Stuart-Williams, H.; Yang, H.; Cao, J. Y.; Luo, W. J.; Li, Z. S.; Liu, Y.; Withers, R. L. *Nat. Mater.* **2010**, *9*, 559−564.
(2) Tong, H.; Ouyang, S. X.; Bi, Y. P.; Umezawa, N.; Oshikiri, M.; Ye, J. H. *Adv. Mater.* **2012**, *24*, 229−251.
(3) Ouyang, S. X.; Tong, H.; Umezawa, N.; Cao, J. Y.; Li, P.; Bi, Y. P.; Zhang, Y. J.; Ye, J. H. *J. Am. Chem. Soc.* **2012**, *134*, 1974−1977.
(4) Tu, W. G.; Zhou, Y.; Liu, Q.; Tian, Z. P.; Gao, J.; Chen, X. Y.; Zhang, H. T.; Liu, J. G.; Zou, Z. G. *Adv. Funct. Mater.* **2012**, *22*, 1215−1221.
(5) Tang, J. W.; Zou, Z. G.; Ye, J. H. *Angew. Chem., Int. Ed.* **2004**, *43*, 4463−4466.
(6) Chen, X.; Liu, L.; Yu, P. Y.; Mao, S. S. *Science* **2011**, *331*, 746−750.
(7) Fujishima, A.; Honda, K. *Nature* **1972**, *238*, 37−38.
(8) Asahi, R.; Morikawa, T.; Ohwaki, T.; Aoki, K.; Taga, Y. *Science* **2001**, *293*, 269−271.
(9) Xiang, Q. J.; Yu, J. G.; Wang, W. G.; Jaroniec, M. *Chem. Commun.* **2011**, *47*, 6906−6908.
(10) Xiang, Q. J.; Yu, J. G.; Jaroniec, M. *J. Am. Chem. Soc.* **2012**, *134*, 6575−6578.
(11) Fujishima, A.; Zhang, X. T.; Tryk, D. A. *Surf. Sci. Rep.* **2008**, *63*, 515−582.
(12) Hernandez-Alonso, M. D.; Fresno, F.; Suarez, S.; Coronado, J. M. *Energy Environ. Sci.* **2009**, *2*, 1231−1257.
(13) Chen, X.; Shen, S.; Guo, L.; Mao, S. S. *Chem. Rev.* **2010**, *110*, 6503−6570.
(14) Chen, J. S.; Tan, Y. L.; Li, C. M.; Cheah, Y. L.; Luan, D. Y.; Madhavi, S.; Boey, F. Y. C.; Archer, L. A.; Lou, X. W. *J. Am. Chem. Soc.* **2010**, *132*, 6124−6130.
(15) Bi, Y. P.; Ouyang, S. X.; Umezawa, N.; Cao, J. Y.; Ye, J. H. *J. Am. Chem. Soc.* **2011**, *133*, 6490−6492.
(16) Jiang, J.; Zhao, K.; Xiao, X. Y.; Zhang, L. Z. *J. Am. Chem. Soc.* **2012**, *134*, 4473−4476.
(17) Pan, J.; Liu, G.; Lu, G. Q.; Cheng, H. M. *Angew. Chem., Int. Ed.* **2011**, *50*, 2133−2137.
(18) Lazzeri, M.; Vittadini, A.; Selloni, A. *Phys. Rev. B: Condens. Matter* **2001**, *63*, 155409.
(19) Liu, S. W.; Yu, J. G.; Jaroniec, M. *J. Am. Chem. Soc.* **2010**, *132*, 11914−11916.
(20) Yang, H. G.; Sun, C. H.; Qiao, S. Z.; Zou, J.; Liu, G.; Smith, S. C.; Cheng, H. M.; Lu, G. Q. *Nature* **2008**, *453*, 638−641.
(21) Barnard, A. S.; Zapol, P.; Curtiss, L. A. *J. Chem. Theory Comput.* **2005**, *1*, 107−116.

(22) Barnard, A. S.; Curtiss, L. A. *Nano Lett.* **2005**, *5*, 1261−1266.
(23) Pan, J.; Wu, X.; Wang, L. Z.; Liu, G.; Lub, G. Q.; Cheng, H. M. *Chem. Commun.* **2011**, *47*, 8361−8363.
(24) Dinh, C. T.; Nguyen, T. D.; Kleitz, F.; Do, T. O. *ACS Nano* **2009**, *3*, 3737−3743.
(25) Kresse, G.; Furthmuller, J. *Comput. Mater. Sci.* **1996**, *6*, 15−50.
(26) Perdew, J. P.; Burke, K.; Ernzerhof, M. *Phys. Rev. Lett.* **1996**, *77*, 3865−3868.
(27) Howard, C. J.; Sabine, T. M.; Dickson, F. *Acta Crystallogr. Sect. B* **1991**, *47*, 462−468.
(28) Ohsaka, T.; Izumi, F.; Fujiki, Y. *J. Raman. Spectrosc.* **1978**, *7*, 321−324.
(29) Gong, X. Q.; Selloni, A. *J. Phys. Chem. B* **2005**, *109*, 19560−19562.
(30) Yang, K.; Dai, Y.; Huang, B. B.; Feng, Y. P. *Phys. Rev. B* **2010**, *81*, 033202.
(31) Yang, H. G.; Liu, G.; Qiao, S. Z.; Sun, C. H.; Jin, Y. G.; Smith, S. C.; Zou, J.; Cheng, H. M.; Lu, G. Q. *J. Am. Chem. Soc.* **2009**, *131*, 4078−4083.
(32) Liu, M.; Piao, L. Y.; Zhao, L.; Ju, S. T.; Yan, Z. J.; He, T.; Zhou, C. L.; Wang, W. J. *Chem. Commun.* **2010**, *46*, 1664−1666.
(33) Liu, G.; Sun, C. H.; Yang, H. G.; Smith, S. C.; Wang, L. Z.; Lu, G. Q.; Cheng, H. M. *Chem. Commun.* **2010**, *46*, 755−757.
(34) Han, X.; Kuang, Q.; Jin, M. S.; Xie, Z. X.; Zheng, L. *J. Am. Chem. Soc.* **2009**, *131*, 3152−3153.
(35) Liu, G.; Yang, H. G.; Wang, X. W.; Cheng, L. N.; Pan, J.; Lu, G. Q.; Cheng, H. M. *J. Am. Chem. Soc.* **2009**, *131*, 12868−12869.
(36) Liu, G.; Sun, C. H.; Smith, S. C.; Wang, L. Z.; Lu, G. Q.; Cheng, H. M. *J. Colloid Interface Sci.* **2010**, *349*, 477−483.
(37) Wang, X. W.; Liu, G.; Wang, L. Z.; Pan, J.; Lu, G. Q.; Cheng, H. M. *J. Mater. Chem.* **2011**, *21*, 869−873.
(38) Zheng, Z. K.; Huang, B. B.; Qin, X. Y.; Zhang, X. Y.; Dai, Y.; Jiang, M. H.; Wang, P.; Whangbo, M. H. *Chem.—Eur. J.* **2009**, *15*, 12576−12579.
(39) Xiang, Q. J.; Yu, J. G.; Jaroniec, M. *Chem. Commun.* **2011**, *47*, 4532−4534.
(40) Yu, J. G.; Qi, L. F.; Jaroniec, M. *J. Phys. Chem. C* **2010**, *114*, 13118−13125.
(41) Lv, K. L.; Yu, J. G.; Fan, J. J.; Jaroniec, M. *CrystEngComm* **2011**, *13*, 7044−7048.
(42) Alivov, Y.; Fan, Z. Y. *J. Phys. Chem. C* **2009**, *113*, 12954−12957.
(43) Zheng, Z. K.; Huang, B. B.; Qin, X. Y.; Zhang, X. Y.; Dai, Y. *Chem.—Eur. J.* **2010**, *16*, 11266−11270.
(44) Ma, X. Y.; Chen, Z. G.; Hartono, S. B.; Jiang, H. B.; Zou, J.; Qiao, S. Z.; Yang, H. G. *Chem. Commun.* **2010**, *46*, 6608−6610.
(45) Chen, J. S.; Tan, Y. L.; Li, C. M.; Cheah, Y. L.; Luan, D.; Madhavi, S.; Boey, F. Y. C.; Archer, L. A.; Lou, X. W. *J. Am. Chem. Soc.* **2010**, *132*, 6124−6130.
(46) Liu, S. W.; Yu, J. G.; Jaroniec, M. *Chem. Mater.* **2011**, *23*, 4085−4093.
(47) Linsebigler, A. L.; Lu, G. Q.; Yates, J. T. *Chem. Rev.* **1995**, *95*, 735−758.
(48) Anpo, M.; Che, M.; Fubini, B.; Garrone, E.; Giamello, E.; Paganini, M. C. *Top. Catal.* **1999**, *8*, 189−198.
(49) Butler, M. A. *J. Appl. Phys.* **1977**, *48*, 1914−1920.
(50) Inoue, T.; Fujishima, A.; Konishi, S.; Honda, K. *Nature* **1979**, *277*, 637−638.
(51) Hoffmann, M. R.; Martin, S. T.; Choi, W. Y.; Bahnemann, D. W. *Chem. Rev.* **1995**, *95*, 69−96.
(52) Ouyang, S. X.; Ye, J. H. *J. Am. Chem. Soc.* **2011**, *133*, 7757.
(53) Vittadini, A.; Selloni, A.; Rotzinger, F. P.; Gratzel, M. *Phys. Rev. Lett.* **1998**, *81*, 2954−2957.
(54) Selloni, A. *Nat. Mater.* **2008**, *7*, 613−615.